Smart Structures and Systems, *Vol. 22, No. 3 (2018) 291-302*
DOI: https://doi.org/10.12989/sss.2018.22.3.291

Damage localization and quantification in beams from slope discontinuities in static deflections

Qiaoyu Ma and Mario Solís*

Department of Continuum Mechanics and Structural Analysis, Escuela Técnica Superior de Ingeniería, Universidad de Sevilla, Camino de los Descubrimientos s/n, 41092 Sevilla, Spain

(Received March 20, 2018, Revised June 8, 2018, Accepted July 3, 2018)

Abstract. This paper presents a flexibility based method for damage identification from static measurements in beam-type structures. The response of the beam at the Damaged State is decomposed into the response at the Reference State plus the response at an Incremental State, which represents the effect of damage. The damage is localized by detecting slope discontinuities in the deflection of the structure at the Incremental State. A denoising filtering technique is applied to reduce the effect of experimental noise. The extent of the damage is estimated through comparing the experimental flexural stiffness of the damaged cross-sections with the corresponding values provided by analytical models of cracked beams. The paper illustrates the method by showing a numerical example with two cracks and an experimental case study of a simply supported steel beam with one artificially introduced notch type crack at three damage levels. A Digital Image Correlation system was used to accurately measure the deflections of the beam at a dense measurement grid under a set of point loads. The results indicate that the method can successfully detect and quantify a small damage from the experimental data.

Keywords: damage identification; static deflection; beams; digital photogrammetry

1. Introduction

Damage detection in structures is based on the identification of the change of structural properties induced by damage. Extensive research on vibration-based damage identification has been developed in the last decades (see Salawu 1997, Doebling *et al*. 1998, Chang *et al*. 2003, Yan *et al*. 2007, Fan and Qiao 2011). For damage detection in beam-type structures, comparative studies on frequency-based and mode-shape-based algorithms have shown that mode-shape-based methods are advantageous for damage localization (see Farrar and Jauregui 1998a, b, Kim *et al*. 2003). Pandey *et al*. (1991) demonstrated that changes in the curvatures of the mode shapes (second-order derivative) reveal the damage location in a beam-like structure and the curvatures of mode shapes are a better indicator for damage localization than the mode shapes. Numerical studies of beams and practical applications in bridges show that the change in curvatures of mode shapes is feasible for multiple damage scenarios detection (see Abdel Wahab and De Roeck 1999, Dawari and Vesmawala 2013, Babu *et al*. 2015). The first-order derivative of mode shapes has also been considered an excellent damage indicator for beams and plates by Abdo and Hori (2002). Higher order derivatives (third and fourth) of beam-like structures have been used for damage localization purpose as well (Whalen 2008). Moreover, other numerical techniques implicitly related to differentiation can be applied to mode shapes for damage localization. For instance, the wavelet transform has been applied to mode shapes (Rucka and Wilde 2006a), curvatures of mode shapes (Cao *et al*. 2014), and changes in mode shapes (Solís *et al*. 2013). Some research studies have also proposed non-baseline methods by using the discontinuities in the derivatives as a damage indicator (see Cao *et al*. 2016, for instance). In the work of Xu *et al*. (2016), they propose the use of slopes in longitudinal displacements by exciting the beam with an axial force.

For dynamic-based methods, the effect of damage is distributed among all modes. However, in practice, the number of modes that can be experimentally identified and analyzed is always limited. For instance, for large-scale structures such as bridges, the higher modes are usually not captured in day-to-day monitoring. This inevitable truncation can lead to damage identification errors (see Abdel Wahab and De Roeck 1999, Babu *et al*. 2015). In contrast, the static response provides more complete and straightforward information about the structural behavior. In addition, data processing for a static test is simpler and less time-consuming than for an experimental modal analysis.

Structural diagnosis techniques that employ static response have been proposed through parameter estimation, solving inverse problem or using strain energy (see Hjelmstad and Shin 1997, Yeo *et al*. 2000, Bakhtiari-Nejad *et al*. 2005, Caddemi and Morassi 2007, Yang and Sun 2010, Seyedpoor and Yazdanpanah 2014). For damage detection in beam-type structures, several methods based on deflection measurements or its derivatives have been presented (see Choi *et al*. 2004, Rucka and Wilde 2006b, Stöhr *et al*. 2006, Abdo 2012). The main difficulty for solving inverse problems of damage detection in beams is that they are usually ill-conditioned. Nonetheless, Caddemi and Morassi (2007) proposed a simple one-dimensional analytical model of cracked beams with typical boundary

*Corresponding author, Assistant Professor
E-mail: msolis@us.es

http://www.techno-press.com/journals/sss&subpage=7 ISSN: 1738-1584 (Print), 1738-1991 (Online)

conditions, such as simply-supported and fixed-fixed, for damage localization. Later, the authors (Caddemi and Morassi 2011) presented a more explicit analytical model for multiple cracks in beams for damage localization and quantification. Choi *et al*. (2004) developed a load theorem that uses the influence line of the moment of the conjugate beam for damage localization in statically determinate beams. Stöhr *et al*. (2006) presented a method using influence lines of slope difference measured by one inclination sensor for damage localization in bridges. Abdo (2012) performed a parametric study on damage localization by applying the Grey Relation Coefficient with the displacement curvature difference.

The main drawback for using the static response is the difficulty in accurately and efficiently measuring the static displacement at a high enough number of measurement points. In Structural Health Monitoring (SHM) application for bridges, various techniques have been developed to measure the static deflection, such as deformation sensors, inclinometers, strain gauges and fiber optic sensors (see Chung *et al*. 2008, Yu *et al*. 2013, Sousa *et al*. 2013). As an alternative, non-contact optical measuring techniques can be used to overcome this issue (Jiang *et al*. 2008). Rucka and Wilde (2006a) used a digital still camera to measure the static displacements of a cantilever beam and applied wavelet analysis directly to the measured data for damage localization.

On the other hand, the problem of a cracked beam under some external static forces can be decomposed into an undamaged state plus an incremental state where a traction field is applied on the crack surface (Gudmundson 1983). Moreover, Caddemi and Morassi (2007) demonstrated the relationship between damage severity and the response of the structure at this incremental state. This paper is also based on this type of decomposition approach. The aim is to develop a fast and robust method for damage identification in beams with cracks through direct experimental measurements without neither solving inverse problems nor estimating any model parameter.

A straightforward and simple damage localization and quantification method that utilizes the static deflection difference between the Reference and Damaged States is proposed. A slope discontinuity in this deflection difference reveals the location of damage. The main concern when dealing with derivatives of experimental mode shapes or static displacements is that they usually can not be directly measured and their computation is subjected to numerical instabilities due to experimental noise. A proper trending filter is proposed in this paper to denoise the data in order to avoid this difficulty. Moreover, the extents of damage can be estimated from the experimentally determined flexural stiffness of the damaged cross-sections.

The rest of the paper is outlined as follows. First, the decomposition scheme and the principle of the method are introduced. Next, the paper presents a general methodology for damage localization and quantification based on the detection of slope discontinuities in the deflection difference between the Reference and the Damaged States. Then, a numerical example is presented to verify the method. Details and performance of the methodology are discussed through an experimental application on simply supported beams with a single crack. Lastly, the conclusions are drawn.

2. Theoretical background

The structural behavior of a cracked beam is a complex problem that has been the subject of many studies over the years. It has been addressed from different perspectives (fracture mechanics, finite element models, experimental tests, etc.) and different parameters have been considered (stress-intensity factors, local flexibility, etc.) (see Dimarogonas 1996). The presence of a crack causes a reduction in the local stiffness of the cross-section. Thus, a damaged cross-section can be macroscopically modeled as a massless rotational spring with a specific stiffness that links the two parts of the beam at both sides of the crack. The ideal lumped model of local stiffness reduction and its vicinity are depicted in Fig. 1.

In the book of Dimarogonas *et al*. (2013), the authors provided correlation equations of the flexural stiffness and the damaged cross-section for different shapes of cross-section and various types of damage. For a notch type opened crack on an elastic beam with a rectangular cross-section, the equivalent flexural stiffness of the damaged cross-section (K_{ana}) can be estimated from Eqs. (1) and (2) (Rizos *et al.* 1990), assuming that the notch has a uniform depth and a sufficient small width to maintain open under loading condition:

$$K_{ana} = 1/c \qquad c = 5.346hJ(\xi)/EI \tag{1}$$

where h is the height of the cross-section, E is the elastic modulus of the material of the beam, I is the moment of inertia of the cross-section, and J is defined by the following function of the ratio ξ between the notch depth and the height of the cross-section.

$$\begin{aligned} J(\xi) = 1.8624(\xi)^2 - 3.95(\xi)^3 + 16.375(\xi)^4 \\ -37.226(\xi)^5 + 76.81(\xi)^6 - 126.9(\xi)^7 \\ +172(\xi)^8 - 143.97(\xi)^9 + 66.56(\xi)^{10} \end{aligned} \tag{2}$$

The problem of a beam with cracks subjected to a general external load is represented from a macro mechanical perspective in Fig. 2.

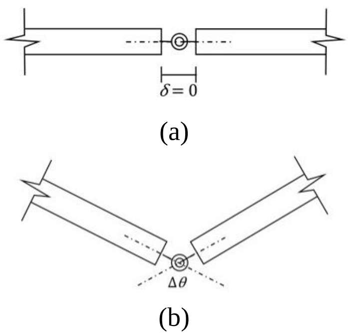

Fig. 1 Ideal lumped damage model: (a) undeformed and (b) deformed

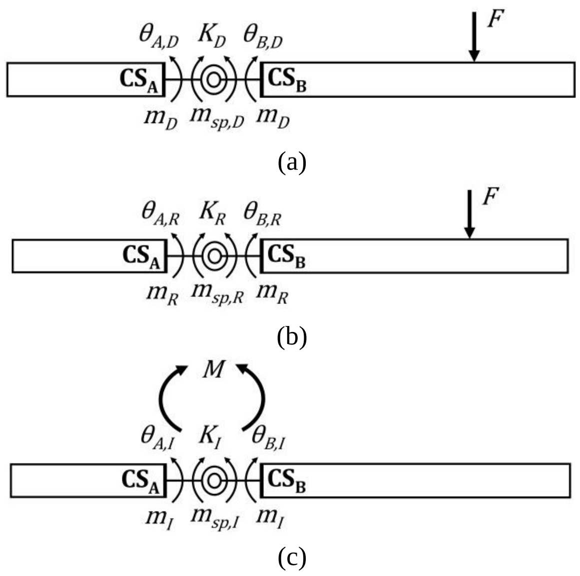

Fig. 2 States of the superposition scheme: (a) Damaged State, (b) Reference State and (c) Incremental State

The damage in the beam is modeled as a massless rotational spring with a stiffness K in the one-dimensional beam model. The beam is under some arbitrary external loads F that can produce non-zero internal moments at damage locations. The external loads remain unchanged after the occurrence of damage. To better demonstrate the scheme, only one single damage is considered in Fig. 2 but the theoretical analysis would be identical for multiple damage scenarios. The response of the structure at Damaged State (State D, Fig. 2(a)) can be understood as the superposition of the response at the Reference State (State R, Fig. 2(b)) plus the effect of applying a certain concentrated self-equilibrated moment, M, at the damage position at the Incremental State (State I, Fig. 2(c)). The presented theory is valid for any boundary conditions that are properly established, i.e., no rigid body motion is allowed and the beam is stable. Therefore, for simplicity and generality, no boundary conditions are specified in Fig. 2. The following list defines the notations plotted in Fig. 2:

Nomenclature

$\mathbf{CS_A}$, $\mathbf{CS_B}$: the cross-sections at the left and right sides of the damage, respectively;

θ_A, θ_B: the rotations of **$\mathbf{CS_A}$** and **$\mathbf{CS_B}$**, respectively;

m: the internal bending moment at **$\mathbf{CS_A}$** and **$\mathbf{CS_B}$** (they are equal to each other because of moment equilibrium at the damage location);

m_{sp}: the internal torsional moment of the spring.

Subscripts *D*, *R* and *I* stand for the Damaged, Reference and Incremental States, respectively.

According to the superposition scheme, the following relationships can be written

$$m_D = m_R + m_I \tag{3}$$

$$m_{sp,D} = m_{sp,R} + m_{sp,I} \tag{4}$$

$$\theta_{A,D} = \theta_{A,R} + \theta_{A,I} \quad \text{and} \quad \theta_{B,D} = \theta_{B,R} + \theta_{B,I} \tag{5}$$

At any state, the constitutive law of the spring states that

$$m_{sp} = K \cdot (\theta_B - \theta_A) \tag{6}$$

At State R, the following compatibility condition is imposed since there is no damage

$$\theta_{A,R} = \theta_{B,R} \tag{7}$$

Thus, Eq. (6) determines that the internal moment of the spring at this state is null

$$m_{sp,R} = K_R \cdot (\theta_{B,R} - \theta_{A,R}) = 0 \tag{8}$$

Eq. (8) implies that the spring has no effect at State R since any value of K_R can satisfy the equation. By subtracting $\theta_{A,D}$ from $\theta_{B,D}$ in Eq. (5), and considering Eq. (7) the following equation is obtained

$$\theta_{B,D} - \theta_{A,D} = \theta_{B,I} - \theta_{A,I} \tag{9}$$

Eqs. (4) and (8) indicate that

$$m_{sp,D} = m_{sp,I} \tag{10}$$

From Eqs. (6), (9) and (10), it is verified that the stiffness of the springs in State D and I are the same

$$K_D = K_I = K \tag{11}$$

At State D, from moment equilibrium, the following equation is obtained

$$m_D = m_{sp,D} \tag{12}$$

At State I, the moment equilibrium can be written as

$$M = m_{sp,I} - m_I \tag{13}$$

Eq. (13) means that the externally applied moment M is partially transmitted to the beam and partially taken by the spring. By introducing Eqs. (3), (10) and (12) in Eq. (13), it is obtained that

$$M = m_R \tag{14}$$

Therefore, in a general situation with multiple damages, the proposed superposition scheme is valid when the external moments applied at State I equal the internal bending moments at damage locations at State R. The applied moments (M) at State I clearly lead to rotational discontinuities between the two sides of the beam connected by the rotational springs. The damage can therefore be localized where the slope discontinuities are identified in the deflection of State I (u_I). According to the superposition scheme, this deflection can be computed from the displacement fields measured at States R (u_R) and D (u_D).

$$u_I = \Delta u = u_D - u_R \tag{15}$$

The flexural stiffness of each cracked section (the rotational stiffness of the springs) can be estimated by applying Eq. (6) to State I

$$K = \frac{m_{sp,I}}{(\theta_{B,I} - \theta_{A,I})} = \frac{m_{sp,I}}{\Delta\theta_I} \tag{16}$$

From Eqs. (10) and (12), Eq. (16) can be written as

$$K = \frac{m_D}{\Delta\theta_I} \tag{17}$$

From the flexural stiffness of the damaged cross-sections, the extents of damage can be assessed by comparing the rotational stiffness estimate with existing correlations. For instance, Eqs. (1) and (2) can be used to estimate the crack depth in a rectangular cross-section. In order to obtain the rotational stiffness from Eq. (17), m_D and $\Delta\theta_I$ at the corresponding damaged cross-section have to be estimated first.

For statically determinate beams, the internal bending moment of the beam at State D can be calculated accurately through structural analysis. For statically indeterminate beams, m_D has to be estimated through numerical analysis or analytical models. The rotation discontinuities can be determined and computed from the deflection difference, as it will be discussed in next sections.

3. Damage identification methodology

3.1 General procedure

The general procedure for damage localization and quantification in beams through experimental measurements is summarized as follows:

1) Measure the static deflections of the structure at States R (u_R) and D (u_D);
2) Compute the deflection increment (Δu) between u_R and u_D using Eq. (15);
3) Compute the value of the slope discontinuities ($\Delta\theta_I$) of Δu and localize damage;
4) Compute the internal bending moment of damaged cross-sections at State D;
5) Compute the flexural stiffness or rotational stiffness (K) at damage locations using Eq. (17);
6) Estimate the damage severity through a previously obtained correlation between damage size and flexural stiffness (such as Eqs. (1) and (2)).

In practice, the corresponding change of the slope in Step 3) can be computed through a finite difference procedure at each measurement point. Given three equally spaced measurement points and their corresponding deflection measurements $[\Delta u(i-1),\ \Delta u(i),\ \Delta u(i+1)]$, the numerical evaluation of the slope difference at point i can be estimated by Eq. (18), where "θ_I^+" and "θ_I^-" are the slope of Δu from forward differencing approach and backward differencing approach, respectively, and Δx is the distance between adjacent measurement points.

$$\begin{aligned}\Delta\theta_I(i) &= \theta_I^+(i) - \theta_I^-(i) \\ &= \frac{\Delta u(i+1) - 2\Delta u(i) + \Delta u(i-1)}{\Delta x}\end{aligned} \tag{18}$$

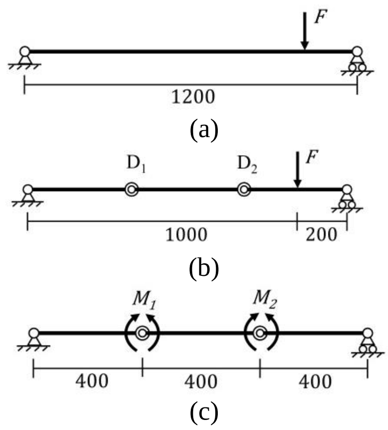

Fig. 3 Scheme of the simply supported beam models: (a) model for State R, (b) model for State D and (c) model for State I (unit: mm)

3.2 Numerical validation

A numerical example with two damages are presented to illustrate the theory of the superposition scheme and the proposed damage detection methodology. A finite element model of a simply-supported one-dimensional Timoshenko steel beam with a length of 1200 mm, a width of 100 mm, a height of 20 mm, and a 200 GPa modulus of elasticity was built. Two springs with equal rotational stiffness, $K_1 = K_2 = 1.8\mathrm{e}^5$ N·m/rad (equivalent to 50% damage severity according to Eqs. (1)-(2)), were used to model two cracked cross-sections (D_1 and D_2). They are located at 1/3 (400 mm) and 2/3 (800 mm) of the beam. A concentrated load, $F = 1000$ N, was applied at 1000 mm from the left end (arbitrarily selected position). The models for States R, D and I are presented in Fig. 3, where M_1 (66.67 N·m) and M_2 (133.33 N·m) equal the internal bending moments at the associated cross-sections at State R.

The deflections of the numerical models of States R and D are shown in Fig. 4(a). It can be seen that there is a difference between the two deflections but there is no evidence of the presence and location of damage from simple inspection. The deflection of State I (u_I) and the deflection increment (Δu) obtained by subtracting u_R from u_D are shown in Fig. 4(b). The consistency of u_I and Δu verifies the superposition scheme presented in Section 2.

In practical applications, in which only measurements of u_D and u_R can be available, the deflection of the Incremental State can be calculated by subtracting u_D and u_R ($\Delta u = u_I = u_D - u_R$). Then, the corresponding slope discontinuities ($\Delta\theta_I$) can be estimated by using Eq. (18). The results in Fig. 4(c) show that the peak values of the rotation difference of the deflection increment reveal the damage locations precisely. The estimates of the damage locations and rotational stiffness of the springs from the deflection difference are listed in Table 1. Neglecting numerical roundup errors, both of the predictions are consistent with the model information.

From this numerical example, the proposed methodology has been verified for damage localization and quantification in noise-free conditions.

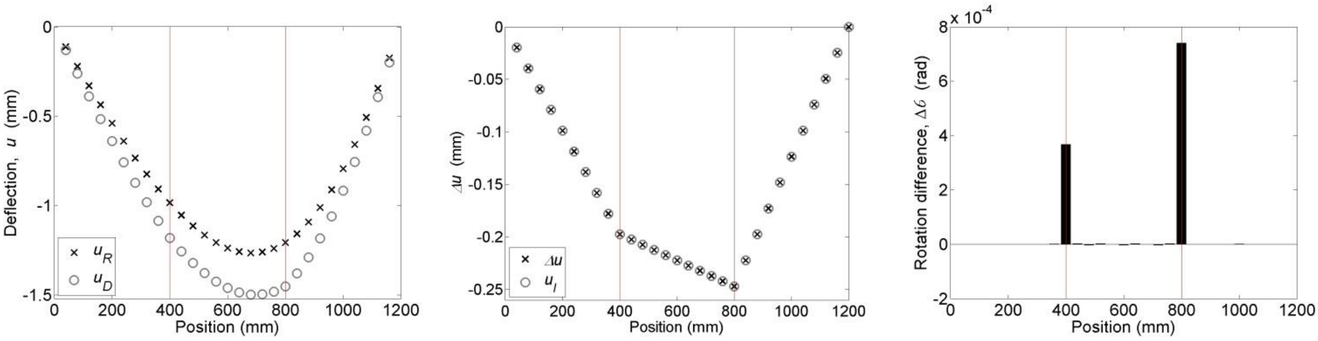

(a) (b) (c)

Fig. 4 (a) Deflections of the finite element model of State R (u_R) and State D (u_D), (b) deflections of the finite element model of State I (u_I) and the difference between u_D and u_R ($\Delta u = u_D - u_R$) and (c) slope difference of Δu. (The red lines mark the damage locations)

Table 1 Numerical results

Damage	Predicted location (mm)	Change in rotation $\Delta\theta$ (rad)	Estimated stiffness K (N·m/rad)
D1	400	$3.68e^{-4}$	$1.81e^{-5}$
D2	800	$7.40e^{-4}$	$1.80e^{-5}$

3.3 Denoising in practical applications

In practical applications, due to the presence of noise, the challenge is to detect and identify the slope discontinuities associated with damage from noisy data. The computation of slope discontinuities can not be done in a straightforward way from the experimental raw data. A denoising function is required to estimate the shape of Δu. In this paper, since many practical implementations of SHM for beam-type structures are of simply supported cases (especially in bridges), details for applying the methodology in this case are provided.

For simply supported beams, the deflection of the beam at State I (Δu) is piecewise linear with turning points at damage locations since the internal forces of undamaged cross-sections at State I are null. Each part of the beam moves as an undeformed rigid body. Therefore, the $l1$ Trending Filter developed by Kim *et al.* (2009) is proposed as a mathematical tool for denoising. The experimentally obtained Δu is treated as a spatially distributed signal and the $l1$ Trending Filter estimates the piecewise linear trend of the data through minimizing the objective function in Eq. (19)

$$\left(\frac{1}{2}\right)\sum_{i=1}^{N}\left(\Delta u(i) - \Delta u_{l1}(i)\right)^2 + \lambda\sum_{i=2}^{N-1}\left|\Delta u_{l1}(i-1) - 2\Delta u_{l1}(i) + \Delta u_{l1}(i+1)\right| \tag{19}$$

where $\Delta u(i)$ is the experimental value of Δu at measurement point i, $\Delta u_{l1}(i)$ is the estimate of the piecewise linear trend at that point, and N is the number of measurement points. λ is a nonnegative parameter which controls the trade-off between the "smoothness" of Δu_{l1} and the residual between the original data (Δu) and the estimated linear trend (Δu_{l1}). As λ approaches 0, Δu_{l1} equals the original data. As λ approaches an upperbound value (λ_{max}), Δu_{l1} is the best linear regression fit (a straight line) of the data. This upperbound value is defined as

$$\lambda_{max} = ||(DD^T)^{-1}D\Delta u||_\infty \tag{20}$$

$$D = \begin{bmatrix} 1 & -2 & 1 & & & \\ & 1 & -2 & 1 & & \\ & & \ddots & \ddots & \ddots & \\ & & & 1 & -2 & 1 \end{bmatrix}_{(n-2)\times n} \tag{21}$$

where $\|\cdot\|_p$ means the pth-norm. It has been proved that λ_{max} can be computed with $O(n)$ arithmetic steps (see Kim *et al.* 2009). The $l1$ Trending Filter can be applied with a Matlab function coded by the authors (Koh *et al.* 2008). Since the value of λ has an influence on how the piecewise linear trend of Δu_{l1} is estimated, it therefore affects the damage localization results. A preliminary inspection on how results are affected by this parameter is necessary in order to select a reasonable value.

A more detailed discussion of the influence of λ and the use of rotation difference in practical applications for damage identification are provided in the experimental study in Section 4.

4. Experimental results

4.1 Test setup

An experimental test of a simply supported steel beam was conducted to test the performance of the methodology. Pictures of the experimental setup and the scheme of the test are shown in Fig. 5. The length of the beam is 1200 mm, and the cross-section is 100 mm wide and 20 mm high. A transversal edge-type notch on the top of the beam at 425 mm from the left end (Fig. 5(a)) was introduced by a saw cut. The depth of the notch is constant through the width of

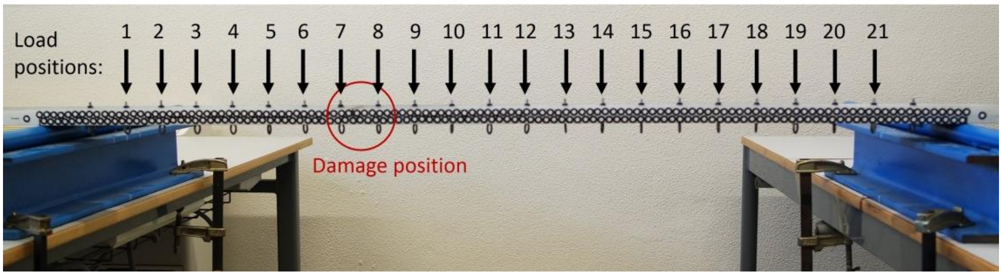

(a)

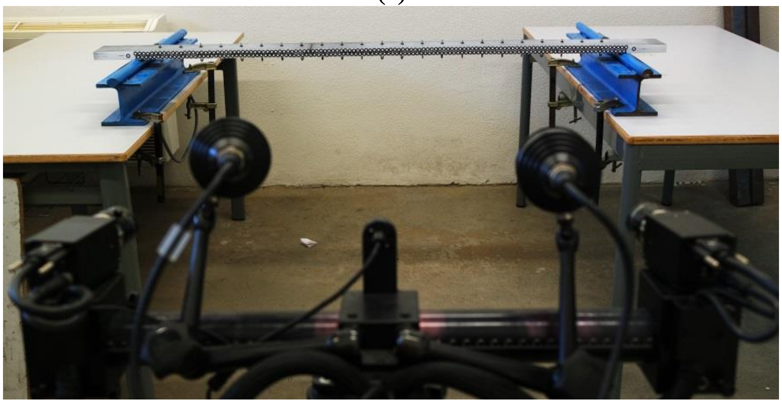

(b)

Fig. 5 Experimental setups: (a) the tested beam and the load positions and (b) the DIC measuring system

the cross-section. Three depths (damage severities) were introduced progressively, 2 mm, 4 mm and 7 mm. They represent 10%, 20% and 35% of the beam height, respectively. It should be noted that, in practice, the depth of the beam is usually higher than its width. However, in the present research, the damage severity is simply defined by the ratio of the crack depth to the beam height and therefore the results are not influenced by the width dimension. The only issue is that the stiffness of the beam is proportional to the width and therefore consistent proportional static loads would be required to obtain the same deflection for different beam widths.

A Digital Imagine Correlation (DIC) system was used to measure the deflection of the beam under static loads (Fig. 5(b)). For each test, 50 images were captured at a sample rate of 1 Hz. Erratic images were discarded and the average values of displacements were computed from the remaining pictures in order to enhance the accuracy of the results. A total number of 241 measurement points were marked along the beam with an equal spacing of 5 mm.

4.2 Static loads

From a theoretical point of view, the method is independent from the distribution and magnitude of the load provided that it produces a non-zero bending moment at damage location. However, in practice, a load that produces a measurable value of deflection increment should be applied. For a single damage case with a concentrated force, the maximum increment is generated by applying the load at the damage location. Therefore, when the damage location is unknown, a distributed load would be preferred rather than a single point load in order to capture a deflection increment as big as possible. However, in practice, a distributed load is more difficult to apply than a concentrated force. One way to approach a distributed load effect is to apply multiple distributed concentrated forces at the same time. The other option is to apply a single concentrated load at multiple positions one at a time and later aggregate the results. In this experimental test, the second method is used. This approach has the advantage of using a small load to obtain a big deflection difference.

A static concentrated force was applied on the beam by hanging a 120 kg mass at 21 equally distributed positions with a spacing of 50 mm (Fig. 5(a)) individually. The static deflection data were stored for both States R and D, respectively. By combining the experimental deflections for each load position (u_j), the resultant value due to a simultaneous application of all the loads (u_{sum}) can be obtained from Eq. (22).

$$u_{sum} = \sum_{j=1}^{21} u_j \tag{22}$$

The measured maximum static deflection of the beam at State R among all load positions is smaller than 4 mm, which is below a usual serviceability limit state requirement. However, the maximum aggregate deflection is 58 mm. This process amplifies the damage effect and therefore can capture small damage effects. Then, these experimental data are processed using the methodology presented in Section 3. The obtained results are presented and discussed in the following sections.

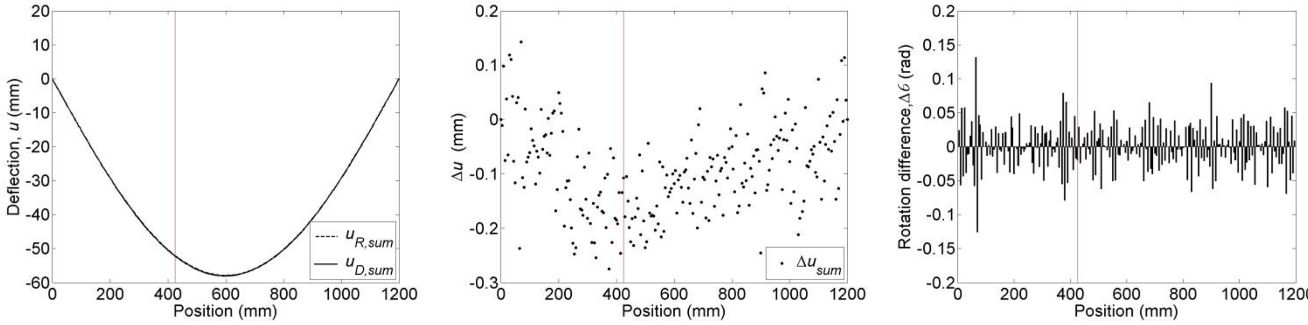

(a) (b) (c)

Fig. 6 Results of direct measurements for 10% severity: (a) the deflection sum at State R ($u_{R,sum}$) and D ($u_{D,sum}$), (b) the difference of the deflections (Δu_{sum}) and (c) the rotation difference of Δu_{sum} ($\Delta\theta$). (The red line marks the actual damage location)

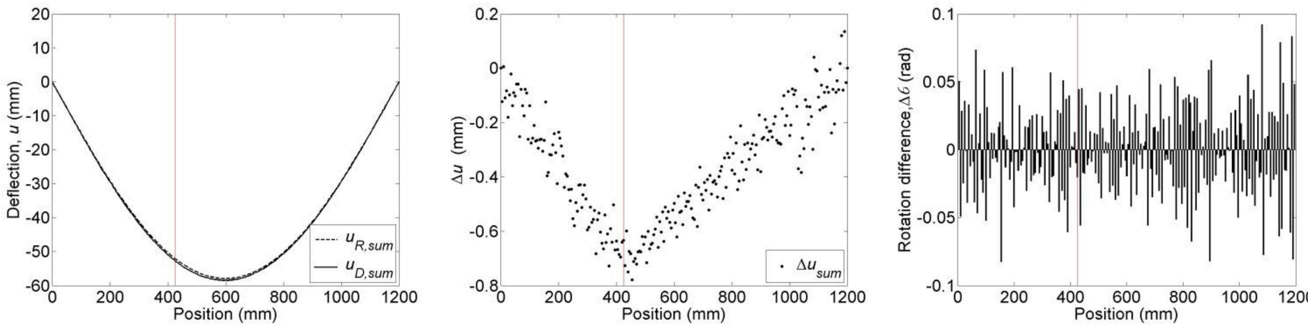

(a) (b) (c)

Fig. 7 Results of direct measurements for 20% severity: (a) the deflection sum at State R ($u_{R,sum}$) and D ($u_{D,sum}$), (b) the difference of the deflections (Δu_{sum}) and (c) the rotation difference of Δu_{sum} ($\Delta\theta$). (The red line marks the actual damage location)

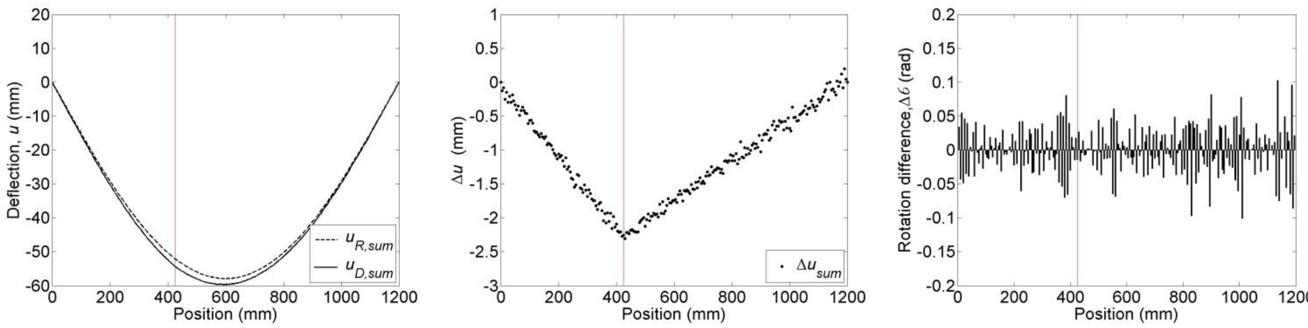

(a) (b) (c)

Fig. 8 Results of direct measurements for 35% severity: (a) the deflection sum at State R ($u_{R,sum}$) and D ($u_{D,sum}$), (b) the difference of the deflections (Δu_{sum}) and (c) the rotation difference of Δu_{sum} ($\Delta\theta$). (The red line marks the actual damage location)

4.3 Raw measurements

The sum of deflections of all load positions at States R and D ($u_{R,sum}$ and $u_{D,sum}$, respectively) are shown in Figs. 6(a), 7(a) and 8(a) for 10%, 20% and 30% damage, respectively. It can be seen that the effects of damage are imperceptible by comparing $u_{R,sum}$ with $u_{D,sum}$ for all three levels of damage. A piecewise linear shape of the deflection differences (Δu_{sum}) that points to damage are observed in Figs. 6(b), 7(b) and 8(b). The trend is more clear for higher damage level due to the decrease of noise level. Nonetheless, the rotation difference of Δu_{sum} computed by using Eq. (18) in Figs. 6(c), 7(c) and 8(c) indicate that the computation of rotation difference directly from raw data is unstable and damage can not be localized even for 35% damage severity. Next, the results with the application of the proposed denoising technique are shown.

4.4 $l1$ Trending filter: Selection of λ

As mentioned in the preceding section, the application of the $l1$ Trending Filter requires a pre-selected value of λ. At this point, the influence of λ should be analyzed in order to obtain good results. The upperbound values for each damage severity are provided in Table 2. Three different λ values defined as a percentage of λ_{max} are considered in this case study (Cases 1, 2 and 3 in Table 2). From Eq. (19), it is intuitive that a higher value of λ/λ_{max} is preferred for higher noise level, and vice versa.

4.5 Identification results

10% Damage

The denoised data from $l1$ Trending Filter ($\Delta u_{sum,l1}$) for 10% damage are plotted in Fig. 9. It is evident that the $l1$ Filter is capable of denoising the experimental data efficiently. For Case 1, Fig. 9(a) shows five clear rotation discontinuities. Three of them are consistent with the sign of their corresponding bending moments whereas the other two are not. Obviously, for a real damage, only a positive value of rotational stiffness from Eq. (17) is meaningful. Therefore, the cross-sections at 180 mm and 950 mm, where rotation differences are inconsistent with the bending moment direction are considered undamaged. For Cases 2 and 3, two and one rotation discontinuities can be observed, respectively.

By comparing the experimental rotational stiffness from Eq. (16) with the analytical value from Eqs. (1) and (2), the estimated crack depths at all measurement points are plotted in Fig. 10. Three damage are identified in Case 1 at 325 mm, 460 mm and 1045 mm with depths of 2.5 mm, 1.3 mm and 4.3 mm, respectively. Fig. 10(b) shows one damage in Case 2 at 330 mm and another at 405 mm. Both estimated crack depths are around 1.6 mm. The only damage in Case 3 is localized at 405 mm with a depth of 2.03 mm. For this damage severity, Case 3 provides the closest identification results to the actual scenario.

Results in Figs. 9(a) and 10(a) indicate that if the value of λ is too small, the $l1$ Trending Filter provides a result close to the original data, which would lead to false positive errors due to its sensitivity to oscillations of the data. The inconsistent rotation discontinuity is an indicator of the inaccuracy of the results of Case 1.

Table 2 Case definition and their corresponding λ values

Case	λ/λ_{max} (%)	Damage severity (%)		
		10	20	35
	100	180.2	732.9	2454.2
1	1	1.8	7.3	24.5
2	10	18	73.3	245.4
3	20	36	146.6	490.8

20% Damage

The denoised data from $l1$ Trending Filter ($\Delta u_{sum,l1}$) for 20% damage in Fig. 11 shows that all three cases of λ provide reasonable estimates of Δu_{sum}. Two rotation discontinuities are observed in Case 1 while only one in Cases 2 and 3. However, Fig. 11(c) illustrates the fact the $l1$ Trending Filter tends to approach the data with a single straight line as λ is higher. Therefore, when λ is too high, the predicted damage location tends to shift towards a wrong location.

The corresponding estimated crack locations and depths are plotted in Fig. 12. Fig. 12(a) shows that one of the two potential damage regions is at 355 mm and the other is from 440 to 455 mm. All estimated crack depths are below 3 mm. In Case 2 (Fig. 12(b)), a single crack is predicted at 440 mm with a 4.3 mm depth. In Case 3, the crack is 4.03 mm deep and is localized at 455 mm. The prediction from Case 2 is 15 mm closer to the actual damage than the prediction from Case 3. Although the evaluated crack depth from Case 2 is 8% higher than the real value, it is considered a very accurate result from a practical point of view. Therefore, for this damage level, Case 2 provides the best damage identification results.

35% Damage

The denoised data from $l1$ Trending Filter ($\Delta u_{sum,l1}$) for 35% damage are plotted in Fig. 13. Apparently, the estimated result from Case 1 matches the raw data better than those from Cases 2 and 3. Figs. 13(b) and 13(c) indicate that both values of λ are too high.

The corresponding estimated crack locations and depths are plotted in Fig. 14. Three consecutive cracks are predicted in Case 1 with the center point at 425 mm. The estimated crack depths are 3.54 mm, 6.57 mm and 3.94 mm, respectively. In Case 2, one single damage is localized at 440 mm with a depth of 7.59 mm (8% overestimated). In Case 3, two adjacent cracks at 450 mm and 455 mm are identified with 1.77 mm and 6.94 mm in depth, respectively. For this damage extent, the prediction from Case 1 is the closest to the actual damage. For this case, the damage is localized with 100% accuracy and the evaluated crack depth is 5% lower than actual value. This difference can be due to the discrepancy between the real crack influence zone and the ideal spring model. On the other hand, although the values of λ are too high for Cases 2 and 3, the results from both cases can be considered very accurate from a practical point of view.

4.6 Analysis of noise level

In this section, the denoised estimate ($\Delta u_{sum,l1}$) is used to evaluate the noise in the raw data (Δu_{sum}). In this discussion, the values of λ that provided the best prediction of the damage are considered. The noise is evaluated by the Coefficient of Variation (CV) defined as

$$\mathrm{CV}_{\%} = \frac{\sigma_{\Delta u_{sum}}}{\mu_{\Delta u_{sum}}} \times 100 \tag{23}$$

where $\sigma_{\Delta u_{sum}}$ and $\mu_{\Delta u_{sum}}$ are the standard deviation and mean value of the sum of deflection difference, defined as

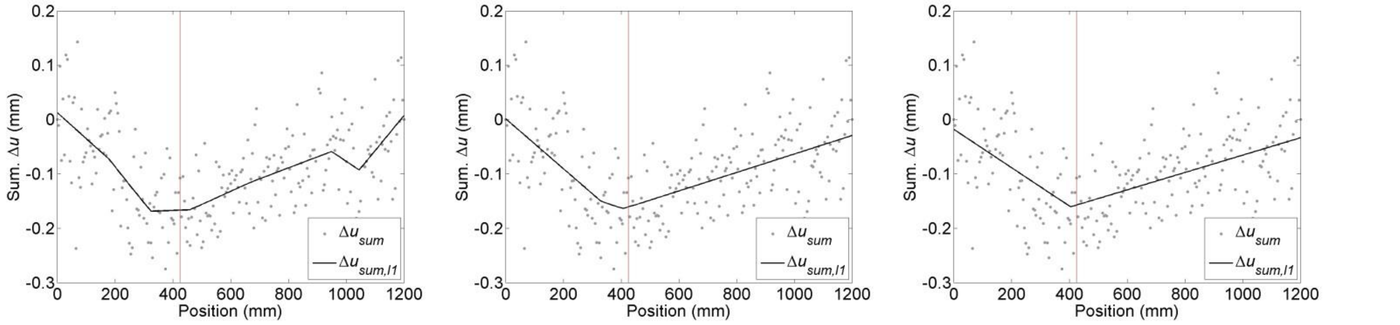

(a) (b) (c)

Fig. 9 Results of $l1$ Trending Filter for 10% damage with different λ: (a) Case 1, (b) Case 2 and (c) Case 3. (The red line marks the actual damage location)

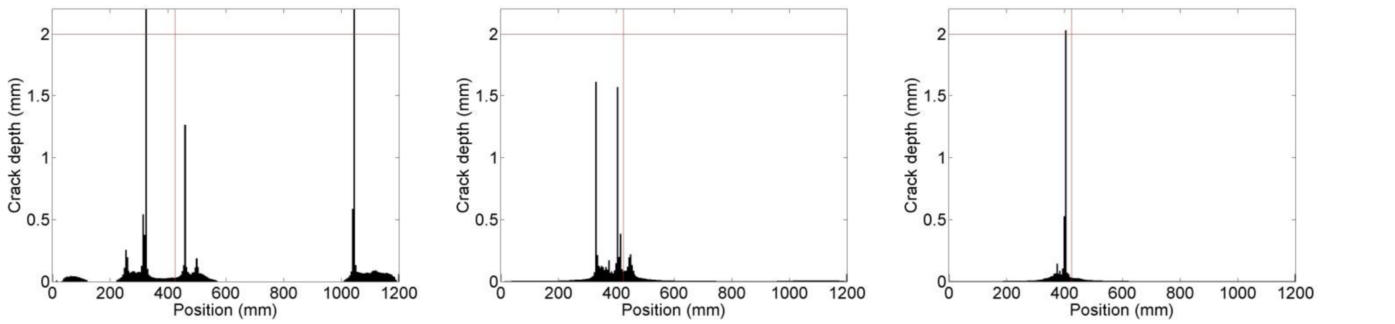

(a) (b) (c)

Fig. 10 Results of estimated crack depth for 10% damage with different λ: (a) Case 1, (b) Case 2 and (c) Case 3. (The red lines mark the actual crack depth and the actual crack location)

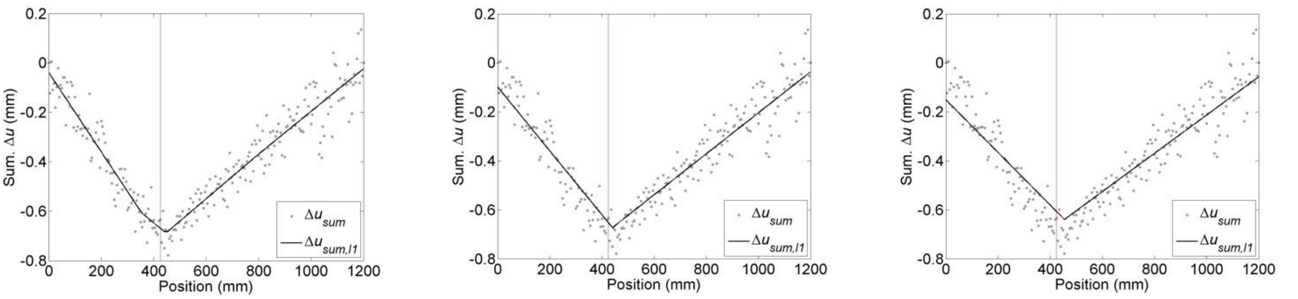

(a) (b) (c)

Fig. 11 Results of $l1$ Trending Filter for 10% damage with different λ: (a) Case 1; (b) Case 2; (c) Case 3. (The red lines mark the actual crack depth and the actual crack location)

$$\sigma_{\Delta u_{sum}} = \sqrt{\frac{1}{N}\sum_{i=1}^{N}(\Delta u_{sum}(i) - \Delta u_{sum,l1}(i))^2} \quad (24)$$

$$\mu_{\Delta u_{um}} = \frac{1}{N}\sum_{i=1}^{N}\Delta u_{sum}(i) \quad (25)$$

being N is the number of measurement points on the beam.

Table 3 Summary of noise evaluation for all damage severities

Damage severity (%)	λ	$\mu_{\Delta u_{sum}}$ (mm)	$\sigma_{\Delta u_{sum}}$ (mm)	CV (%)
10	Case 3	0.0943	0.0671	71
20	Case 2	0.3652	0.0696	19
35	Case 1	1.1305	0.0652	6

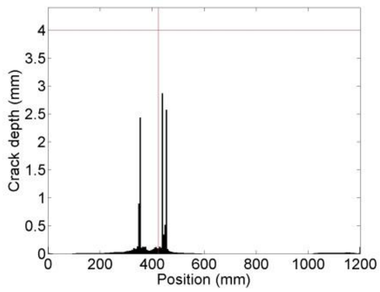
(a)
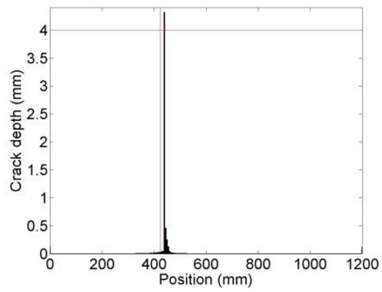
(b)
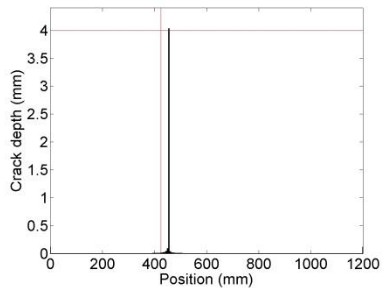
(c)

Fig. 12 Results of estimated crack depth for 20% damage with different λ: (a) Case 1, (b) Case 2, (c) Case 3. (The red lines mark the actual crack depth and the actual crack location)

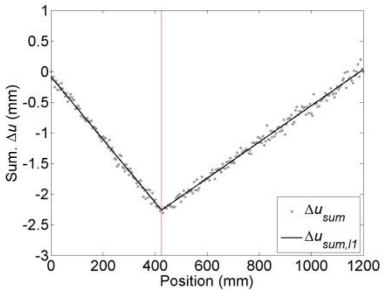
(a)
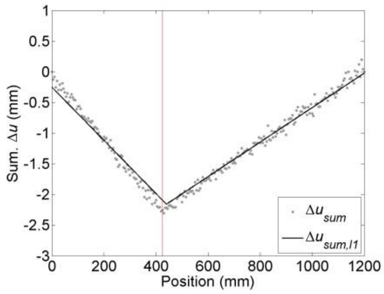
(b)
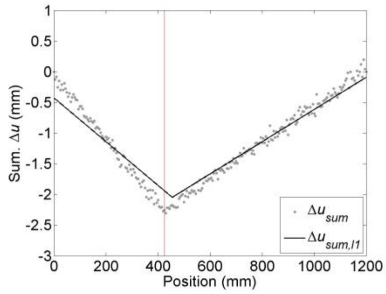
(c)

Fig. 13 Results of $l1$ Trending Filter for 35% damage with different λ: (a) Case 1, (b) Case 2, (c) Case 3. (The red lines mark the actual crack depth and the actual crack location)

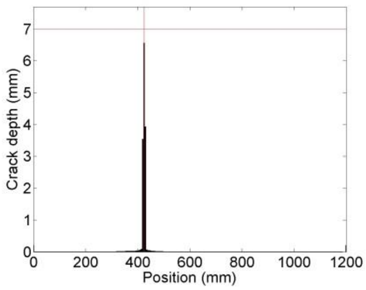
(a)
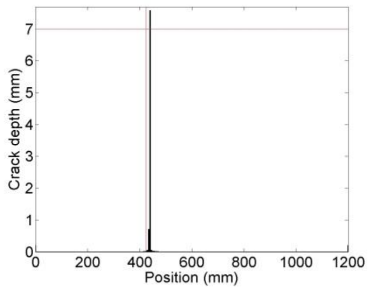
(b)
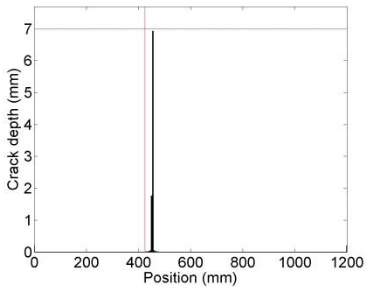
(c)

Fig. 14 Results of estimated crack depth for 35% damage with different λ: (a) Case 1, (b) Case 2, (c) Case 3. (The red lines mark the actual crack depth and the actual crack location)

Table 4 Summary of closest prediction for all damage severities

Damage severity (%)	λ	Predicted locations (mm)	Estimated depth (mm)
10	Case 3	405	2.03
20	Case 2	440	4.32
35	Case 1	425	6.57

Table 3 shows that, the standard deviations of deflection difference for all three damage levels are similar, which indicates that the accuracy of the measuring system is consistent for all the tests. The experimental noise is mainly caused by the resolution accuracy of the DIC measuring system. However, as the damage severity grows, the noise level expressed by the CV decreases significantly. As a result, the damage identification is more reliable.

4.7 Summary

In this case study, three λ values corresponding to 1%, 10% and 20% of λ_{max} are investigated for three levels of damage severity (depth of 10%, 20% and 35% of cross-section height). The best assessment results for all damage scenarios are listed in Table 4. For different damage levels, the best choice of λ varies. Despite the measurements are highly contaminated by noise for 10% damage, the methodology successfully localizes and quantifies the damage. As the damage level increases, a smaller portion of λ_{max} performs better for the damage identification process. When the value of λ is too small (see Case 1 for 10% damage Figs. 6(a) and 10(a)), the effect of noise could lead to false positive errors and unrealistic results. On the other hand, when the value of λ is too high, the denoising method tends to provide inaccurate damage estimation results. When λ is properly selected, the accuracy of both the localization and quantification results are improved.

The results in Case 2 for 10% damage (see Fig. 10(b)) and Case 1 for 20% damage (see Fig. 12(a)) illustrate a similar phenomenon. A multiple damage scenario with two cracks close to the actual damage location can be identified from the peaks on the estimated rotation difference. This is due to an improper value of λ. However, the estimate of the deflection increment ($\Delta u_{sum,l1}$) seems to be well correlated with the original noisy data (Δu_{sum}) in Figs. 9(b) and 11(a), respectively. The fact that the estimated multiple damages are of a lower severity than the actual single crack can be regarded as the non-uniqueness of the solution in solving the inverse problem of damage identification from the estimate of the deflection increment ($\Delta u_{sum,l1}$). In other words, the effect of an actual single damage can be equivalent to that of multiple damages with lower severities near its location. Thus, results from these two cases can be considered also valid from a practical point of view. On the other hand, cross-sections with very small values of estimated crack depths in Figs. 10, 12 and 14 are considered undamaged in practical applications.

5. Conclusions

A damage detection and localization method in beams based on the changes in static deflections is presented in this paper. The discontinuities in the slope of the deflection difference between the pre- and post-damage states of the beam reveal the damage locations. Moreover, through theory of mechanics, the damage severities of the damaged cross-sections can be estimated. The merits of the proposed methodology are summarized as follows:

- It is efficient and simple to implement in practical applications;
- It is non-modelled based for damage detection and localization;
- It is a promising robust to noise approach;
- Theoretically, even the deflections induced by a permanent dead load on the structure could be used.

The proposed methodology has been validated by experimental test with various severities of damage. Although at this moment, the selection of λ is based on trial and error, the authors note that a range between 1 to 20% of the maximum value would be a good initial point. The performance of the proposed methodology for multiple damage scenarios is under investigation. Questions such as the sensitivity of the method to relative damage severity and the minimum perceptible damage spacing are being studied. Moreover, specific denoising methodologies for other types of boundary conditions will be explored.

Acknowledgments

This work was supported by the Consejería de Economía, Innovación, Ciencia y Empleo of Andalucía (Spain) under project P12-TEP-2546 and the Spanish Ministry of Economy and Competitiveness (Ministerio de Economía y Competitividad, Secretaría de Estado de Investigación, Desarrollo e Innovación) through research project BIA2016-43085-P. The financial support is gratefully acknowledged.

References

Abdel Wahab, M.M. and De Roeck, G. (1999), "Damage detection in bridges using modal curvatures: application to a real damage scenario", *J. Sound Vib.*, **226**, 217-235.

Abdo, M.A.B. (2012), "Parametric study of using only static response in structural damage detection", *Eng. Struct.*, **34**, 124-131.

Abdo, M.A.B. and Hori, M. (2002), "A numerical study of structural damage detection using changes in the rotation of mode shapes", *J. Sound Vib.*, **251**, 227-239.

Babu, K.R.P., Kumar, B.R., Narayana, K.L. and Rao, K.M. (2015), "Multiple crack detection in beams from the differences in curvature mode shapes", *APRN J. Eng. Appl. Sci.*, **10**, 1701-1710.

Bakhtiari-Nejad, F., Rahai, A. and Esfandiari, A. (2005), "A structural damage detection method using static noisy data", *Eng. Struct.*, **27**, 1784-1793.

Caddemi, S. and Morassi, A. (2011), "Detecting multiple open cracks in elastic beams by static tests", *J. Eng. Mech.*, **137**, 113-124.

Caddemi, S. and Morassi, A. (2007), "Crack detection in elastic beams by static measurements", *Int. J. Solids Struct.*, **44**, 5301-5315.

Cao, M., Radzieński, M., Xu, W. and Ostachowicz, W. (2014), "Identification of multiple damage in beams based on robust curvature mode shapes", *Mech. Syst. Signal Pr.*, **46**, 468-480.

Cao, M.S., Xu, W., Ren, W.X., Ostachowicz, W., Sha, G.G. and Pan, L.X. (2016), "A concept of complex-wavelet modal curvature for detecting multiple cracks in beams under noisy conditions", *Mech. Syst. Signal Pr.*, **76-77**, 555-575.

Chang, P.C., Flatau, A. and Liu, S.C. (2003), "Review paper: Health monitoring of civil infrastructure", *Struct. Health. Monit.*, **2**, 257-267.

Choi, I.Y., Lee, J.S., Choi, E. and Cho, H.N. (2004), "Development of elastic damage load theorem for damage detection in a statically determinate beam", *Comput. Struct.*, **82**, 2483-2492.

Chung, W., Kim, S., Kim, N.S. and Lee, H. (2008), "Deflection estimation of a full scale prestressed concrete girder using long-gauge fiber optic sensors", *Constr. Build. Mater.*, **22**, 394-401.

Dawari, V.B. and Vesmawala, G.R. (2013), "Structural damage identification using modal curvature differences", *IOSR-JMCE* 33-38.

Dimarogonas, A.D. (1996), "Vibration of cracked structures: A state of the art review", *Eng. Fract. Mech.*, **55**, 831-857.

Dimarogonas, A.D., Paipetis, S.A. and Chondros, T.G. (2013),

Analytical Methods in Rotor Dynamics, (2nd Ed.), Springer.
Doebling, S.W., Farrar, C.R. and Prime, M.B. (1998), "A summary review of vibration-based damage identification methods", *Shock Vib. Dig.*, **30**, 91-105.
Fan, W. and Qiao, P. (2011), "Vibration-based damage identification methods: A review and comparative study", *Struct. Health. Monit.*, **10**, 83-111.
Farrar, C.R. and Jauregui, D.A. (1998a), "Comparative study of damage identification algorithms applied to a bridge: I. Experiment", *Smart Mater. Struct.*, **7**, 704-719.
Farrar, C.R. and Jauregui, D.A. (1998b), "Comparative study of damage identification algorithms applied to a bridge: II. Numerical study", *Smart Mater. Struct.*, **7**, 720-731.
Gudmundson, P. (1983), "The dynamic behaviour of slender structures with cross-sectional cracks", *J. Mech. Phys. Solids*, **31**, 329-345.
Hjelmstad, K.D. and Shin, S. (1997), "Damage detection and assessment of structures from static response", *J. Eng. Mech.*, **123**, 568-576.
Jiang, R., Jáuregui, D.V. and White, K.R. (2008), "Close-range photogrammetry applications in bridge measurement: Literature review", *Measurement*, **41**, 823-834.
Kim, J.T., Ryu, Y.S., Cho, H.M. and Stubbs, N. (2003), "Damage identification in beam-type structures: frequency-based method vs mode-shape-based method", *Eng. Struct.*, **25**, 57-67.
Kim, S.J., Koh, K., Boyd, S. and Gorinevsky, D. (2009), "*l*1Trend filtering", *SIAM Rev.*, **51**, 339-360.
Koh, K., Kim, S.J. and Boyd, S. (2008), Software for *l*1 Trending Filtering, https://stanford.edu/~boyd/l1_tf/.
Pandey, A.K., Biswas, M. and Samman, M.M. (1991), "Damage detection from changes in curvature mode shapes", *J. Sound Vib.*, **145**, 321-332.
Rizos, P.F., Aspragathos, N. and Dimarogonas, A.D. (1990), "Identification of crack location and magnitude in a cantilever beam from the vibration modes", *J. Sound Vib.*, **138**, 381-388.
Rucka, M. and Wilde, K. (2006a), "Application of continuous wavelet transform in vibration based damage detection method for beams and plates", *J. Sound Vib.*, **297**, 536-550.
Rucka, M. and Wilde, K. (2006b), "Crack identification using wavelets on experimental static deflection profiles", *Eng. Struct.*, **28**, 279-288.
Salawu, O.S. (1997), "Detection of structural damage through changes in frequency: a review", *Eng. Struct.*, **19**, 718-723.
Seyedpoor, S.M. and Yazdanpanah, O. (2014), "An efficient indicator for structural damage localization using the change of strain energy based on static noisy data", *Appl. Math. Model.*, **38**, 2661-2672.
Solís, M., Algaba, M. and Galvín, P. (2013), "Continuous wavelet analysis of mode shapes differences for damage detection", *Mech. Syst. Signal Pr.*, **40**, 645-666.
Sousa, H., Cavadas, F., Henriques, A., Bento, J. and Figueiras, J. (2013), "Bridge deflection evaluation using strain and rotation measurements", *Smart Struct. Syst.*, **11**(4), 365-386.
Stöhr, S., Link, M., Rohrmann, R. and Rücker, W. (2006), "Damage detection based on static measurements of bridge structures", *Proceedings of the Int. Modal Anal. Conf. IMAC XXIV*, Orlando, United States, Feburary.
Whalen, T.M. (2008), "The behavior of higher order mode shape derivatives in damaged, beam-like structures", *J. Sound Vib.*, **309**, 426-464.
Xu, W., Zhu, W.D., Smith, S.A. and Cao, M.S. (2016), "Structural damage detection using slopes of longitudinal vibration shapes", *J. Vib. Acoust.*, **138**, 034501.
Yan, Y.J., Cheng, L., Wu, Z.Y. and Yam, L.H. (2007), "Development in vibration-based structural damage detection technique", *Mech. Syst. Signal Pr.*, **21**, 2198-2211.
Yang, Q.W. and Sun, B.X. (2010), "Structural damage localization and quantification using static test data", *Struct. Health. Monit.*, **10**, 381-389.
Yeo, I., Shin, S., Lee, H.S. and Chang, S. (2000), "Statistical damage assessment of framed structures from static responses", *J. Eng. Mech.*, **126**, 414-421.
Yu, Y., Liu, H., Li, D., Mao, X. and Ou, J. (2013), "Bridge deflection measurement using wireless mems inclination sensor systems", *Int. J. Smart Sens. Intell. Syst.*, **6**, 38-57.

HJ